DOI：10. 11714/acta. snus. ZR20250226

Morphological changes and gibberellin-related gene expression patterns during fruit growth and development of *Amomum villosum*[*]

LÜ Bingding[1], *ZHANG Yuyi*[1,2], *TANG Liyun*[3], *HU Jiajia*[1,4], *SU Jing*[5], *XU Jie*[1,6], *HE Zhuohang*[1,7], *HE Guozhen*[1]✉

1. *School of Chinese Materia Medica, Guangzhou University of Chinese Medicine, Guangzhou 510006, China*
2. *The College of Natural Resources and Environment, South China Agricultural University, Guangzhou 510642, China*
3. *College of Life Sciences, South China Agricultural University, Guangzhou 510642, China*
4. *Department of Pharmacy, Fengcheng People's Hospital, Fengcheng 331100, China*
5. *Agricultural Experiment Farm of Yangchun City (Amomum villosum Testing Farm of Yangchun City), Yangchun 529600, China*
6. *Guangdong Yifang Pharmaceutical Co., Ltd. / Guangdong Provincial Key Laboratory of Traditional Chinese Medicine Formula Granule, Foshan 528244, China*
7. *DaAn Gene Co., Ltd., Guangzhou 510665, China*

Abstract: The fruit of *Amomum villosum* is highly valued for its medicinal and edible properties. However, the fruit abscission rate is exceptionally high, resulting in low unit yield. To better understand the fruit growth and development, this study investigated the characteristic changes of fruits and the expression patterns of GA-related genes in both fruits and fruit stalks. Results revealed that it takes approximately 90 days for the ovary of *A. villosum* to reach maturity. Fruit growth pattern exhibited a slow-fast-slow trend, with the peak of fruit weight accumulation occurring between the 14 and 25 days after artificial pollination (DAP). Before the 27 DAP, significant changes were observed in the ovary, fruit color, pericarp thickness, and fruit thorn length. Additionally, ten candidate GA-related genes, including 1 *$GA_{13}ox$*, 1 *$GA_{20}ox$*, 1 *GA_3ox*, 2 *GA_2oxs*, 4 *GID1cs*, and 1 *DELLA*, were analyzed using bioinformatics tools. The GA-related genes in fruit and fruit stalk exhibited significant correlations with fruit growth/development and fruit dropping. Overall, the fruit growth and development law, and the expression patterns of GA-related genes provided a theoretical foundation for further functional study and the screening of candidate genes for potential applications in *A. villosum*.

Key words: *Amomum villosum*; gibberellin; fruit development; gene expression pattern; bioinformatic
CLC number: Q94　**Document code:** A　**Article ID:** 2097 − 0137(XXXX)XX − 0001 − 14

* **Received**: 2025 − 10 − 20　**Accepted**: 2025 − 11 − 09　**Published online**: 2025 − 12 − XX
Supported by Seed Industry Vitalization Project of Rural Revitalization Strategy of Guangdong Province of China (2024-440000-90060000-8796)

✉ **Corresponding author**: HE Guozhen (*heguozhen@gzucm.edu.cn*)
LÜ Bingding (*20232110068@stu.gzucm.edu.cn*); ZHANG Yuyi (*2454567366@qq.com*); TANG Liyun (*tly1231@scau.edu.cn*); HU Jiajia (*1015850392@qq.com*); SU Jing (*573553847@qq.com*); XU Jie (*935394848@qq.com*); HE Zhuohang (*775900345@qq.com*)

增强出版　全文阅读
ZR20250226　ZR20250226

Amomum villosum, a well-documented traditional Chinese medicinal plant, has been used for over a thousand years to treat gastrointestinal disorders (Chen, 2010). It is a perennial evergreen herbaceous plant belonging to the genus *Amomum* in the family *Zingiberaceae* characterized by erect stems reaching 1−3 m in height, with leaves arranged alternately along the aerial axis. This species develops stoloniferous rhizomes forming a networked growth system through which multiple erect stems remain interconnected (de Boer et al. , 2018). *A. villosum* produces spike inflorescences from stoloniferous rhizomes that creep along the soil surface, propagating through both sexual reproduction via seeds and clonal expansion through vegetative rhizome proliferation. It typically requires 2−3 years of growth post-planting to initiate flowering and fruiting phases. *A. villosum* is predominantly distributed in tropical and subtropical monsoon climate regions, where it primarily inhabits shaded understory environments within forest ecosystems (Han et al. , 1984; Guo et al. , 2016). Ecologically, *A. villosum* demonstrates a preference for environments with diffused light exposure, sustained warm temperatures, and high atmospheric humidity (Feng et al. , 2007). The species exhibits physiological constraints including low tolerance to direct solar radiation, drought stress, and waterlogged soil conditions, with optimal growth observed in well-drained, humus-rich substrates (Xu et al. , 2018).

The dried ripe fruits of *A. villosum*, termed ShaRen (a traditional Chinese medicinal name), constitute the primary medicinal organ of this species and are extensively employed in traditional Chinese medicine (TCM) formulations due to their therapeutic properties, such as anti-inflammatory and gastroprotective effects (Huang et al. , 2020). The main components in *A. villosum* include terpenoids, saponins, flavonoids, and polysaccharides (Li et al. , 2024). Its dried fruits can also be used as food, dietary supplements, and spices. The cultivation areas of authentic ShaRen medicinal material is located at Yangchun City, Xinxing County, Gaozhou City and Xinyi City, Guangdong Province (Huang et al. , 2020). However, *A. villosum* suffers from severely low yields in cultivation, which is predominantly attributed to excessive physiological fruit abscission during its fruit development. While our preliminary studies have characterized thetemporal pattern of fruit abscissionand identified elevated gibberellic acid (GA_3) levels in the stalks of normal fruits, the physiological dynamics underlying its fruit growth trajectories and abscission-related hormonal regulation remain poorly characterized, limiting targeted strategies to mitigate yield loss (LÜ et al. , 2021). Therefore, elucidating the GA-related molecular network during fruit development is crucial for addressing the yield bottleneck.

The phytohormone gibberellins (GA), tetranuclear diterpenoids, impact almost every aspect of plant growth and development (Hedden, 2020), such as seed germination (Peng et al. , 2003; Xu et al. , 2023), stem and leaf growth (Wang et al. , 2017), induction of floral organs (Zhang et al. , 2023; Liu et al. , 2023) and fruit growth (Liu et al. , 2018). To date, 136 GAs have been discovered and sequentially designated as GA_1 to GA_{136}. Among these, GA_1, GA_3, GA_4 and GA_7 are regarded as bioactive gibberellins, while the others are non-bioactive. The latter typically serve as precursors or metabolites in GA biosynthesis pathway (Gao et al. , 2020).

In plant, GAs are synthesized through multiple enzymatic reactions (Binenbaum et al. , 2018). The first reaction occurs in the plastid, where geranylgeranyl diphosphate (GGDP) is catalyzed into ent-kaurene by ent-copalyl diphosphate synthase (CPS) and ent-kaurene synthase (KS) (Yamamura et al. , 2018). In the second stage, ent-kaurene is converted to GA_{12} on the endoplasmic reticulum membrane, catalyzed by ent-kaurene oxidase (KO) and ent-kaurenoic acid oxidase (KAO) (Su et al. , 2016). In the third stage, various GAs are synthesized via the action of GA_{13}-oxidase, GA_{20}-oxidase, GA_3-oxidase, GA_2-oxidase (Yamaguchi, 2008). Subsequently, bioactive GAs bind to Gibberellin Insensitive Dwarf1 (GID1), the resulting complex binds to the N-terminus of DELLA proteins, and then the SLY1 subunit of the SCF^{SLY1} complex binds to the GRAS domain at the C-terminus of DELLA proteins, inducing the degradation of DELLA proteins through

the 26S proteasome pathway (Xiang et al. , 2018). With the suppression of DELLA proteins relieved, GAs initiate the regulation of plant growth (Phokas et al. , 2021).

Fruit growth and development are regulated by GAs (Hu et al. , 2018). The transformation of the ovary into fruit is often dependent on ovule fertilization (Gillaspy et al. , 1993). Traditionally, it is believed that following fertilization, the production of endogenous auxin signals activates GA synthesis to regulate fruit set (Fenn et al. , 2021; Seymour et al. , 2014). In watermelon, after pollination, the transcription levels of numerous auxin-related genes in the ovary are upregulated, alongside the upregulation of *$GA_{20}ox$* and *GA_3ox* and downregulation of *GA_2ox*; endogenous IAA content gradually increases post-pollination, with GA_4 content peaking on the 3 DAP (Hu et al. , 2019). In tomatoes, the expression level of *$GA_{20}ox$* in pollinated ovaries is significantly higher than that in unpollinated ovaries, while *GA_2ox* gene expression show no significant change—this may promote the synthesis of bioactive GAs (Carlos et al. , 2007). Tomato *gib1, 2, 3* mutant fail to set fruit normally but recover following GA treatment (Ariizumi et al. , 2013). After fruit set, cell division and elongation are accelerated (Seymour et al. , 2014). Overexpression of *GA_2ox1* in tomatoes reduces the expression of cell expansion-related genes, leading to decreased cell volume, fruit weight, seed number, and seed germination rate; however, exogenous application of GA_3 post-pollination can alleviate these effects (Chen et al. , 2016). During the transition from cell division to cell elongation in wild strawberry fruits, *DELLA* expression decreases (Csukasi et al. , 2011); fruits treated with auxin become plump, while those treated with GA show obvious elongation (Liao et al. , 2018). Once the rapid growth stage ends, the fruit enters the maturation phase. Higher GA content delays fruit ripening (Alferez et al. , 2021; Bai et al. , 2021).

Fruit abscission is regulated by a complex phytohormone network (Taylor et al. , 2001; Estornell et al. , 2013). GAs play important biological roles in regulating fruit abscission, but the effect of GAs on abscission varies among different plant species (Xie et al. , 2018; Reig et al. , 2018). Some researchers found that exogenous application of GA_3 in grapes upregulates the expression of the lignin synthesis gene *VvCAD1*, leading to severe lignification of fruit stalks, increased brittleness, easier fracture of fruit stalks, and a higher fruit abscission rate (García-Rojas et al. , 2018). The citrus huanglongbing-resistant variety 'LB8-9' exhibits a low fruit drop rate and low expression level of *GA_2ox* at the abscission zone, which may ensure sufficient endogenous bioactive GAs to prevent fruit abscission (Tang et al. , 2020).

Our previous study revealed that GA_3 content in the stalks of normal fruits is significantly higher than that in abscission-prone stalks (LÜ et al. , 2021). However, the expression patterns of GA-related genes during fruit growth and development remain uncharacterized. In this study, we investigated the fruit characteristics of *A. villosum* at different developmental stages, cloned key genes involved in GA biosynthesis and signal transduction pathways, and analyzed the expression levels of these genes across various fruit developmental stages. This study delineates the pattern of fruit growth and development and the expression profiles of GA-related genes during fruit development, establishing a theoretical foundation for future functional studies on *A. villosum*.

1 Materials and methods

1. 1 Plant material

A. villosum plants were cultivated in a ShaRen planting base located in Yangchun City, Guangdong Province, China. Normal fruits and fruit stalks were collected at different days after pollination (DAP). The classification criteria for normal fruits and abscised fruits, as well as sampling time points, were adapted from LÜ et al. (2021), with modifications tailored to the developmental stages of *A. villosum* fruits.

For fruit growth analysis, normal fruits were collected at 0, 1, 3, 6, 9, 12, 15, 18, 21, 24, 27, 30, 45, 60, 75 and 90 DAP. To capture critical molecular transitions, normal fruits were also collected at 0, 6, 12, 18, 24, 30, 45, 60, 75, 90 DAP. Normal fruit stalks were specifically collected at 0, 6, 12, 18, 24,

30 DAP (primary abscission phase). All normal fruits and fruit stalks used for gene cloning and expression analysis were flash-frozen in liquid nitrogen and stored at −80 ℃ until subsequent analysis.

1. 2 Morphological measurement

To characterize the morphological changes of fruits during growth and development, fresh fruits were collected at different DAP. A Canon EOS 30D digital camera was used to record fruit shape and color. An Olympus SZ61 stereomicroscope coupled with the MShot Image Analysis System was employed to capture the longitudinal/transverse section anatomy of fruits, as well as to measure fruit longitudinal diameter (FLD), fruit transverse diameter (FTD), fruit peel thickness (FPT), fruit thorn length (FTL), and seed shape, color, and size. A Sartorius CP423S analytical balance was used to determine the weight of individual fruits and seed clusters (Supply: Appendix fig. 2−5).

1. 3 RNA extraction

Total RNA from fruits and fruit stalks at 0−30 DAP was extracted using the Plant Total RNA Isolation Kit (Sangon Biotech, Shanghai, China), while total RNA from fruits at 45−90 DAP was extracted using the OminiPlant RNA Kit (CWBIO, Jiangsu, China), following the manufacturers' protocols. RNA integrity was verified using an ultraviolet (UV) spectrophotometer (Thermo, Massachusetts, USA). RNA samples with an A_{260}/A_{280} ratio of 1. 8−2. 2 were used for subsequent analyses.

1. 4 Identification of candidate GA-related genes

To identify genes involved in GA biosynthesis and signal transduction pathways, we retrieved previously characterized GA-related protein sequences from other plant species from the NCBI database (query sequence IDs are listed in Supply: Appendix table 3). Their homologs in the *A. villosum* transcriptome database were identified using local BLASTp in BioEdit software, with the following selection criteria: Alignment score > 100, similarity identity ⩾ 40%, comparison length ⩾ 50 %, sequence length > 800 bp and E value ⩽ e^{-6}.

1. 5 Cloning of the full-length cDNA sequences of GA-related genes

cDNA fragments were obtained using the Evo M-MLV One Step RT-PCR Kit (Accurate Biology, Hunan, China) following the manufacturer's protocol. The one-step RT-PCR conditions were as follows: 50 ℃ for 30 min, 94 ℃ for 5 min, followed by 35 cycles of 94 ℃ for 30 s, 52−62 ℃ for 30 s, and 72 ℃ for 2 min, with a final extension at 72 ℃ for 5 min. The RT-PCR products were verified by agarose gel electrophoresis, and the target bands were recovered and sequenced.

RACE-PCR primers were designed based on the above sequencing results. The 3' and 5' cDNA libraries were constructed using the SMART RACE Technology Kit (TaKaRa, Dalian, China) according to the manufacturer's instructions. The PCR reaction system and vector construction were performed as previously described (Zhao et al. , 2021), using PrimeSTAR Max DNA Polymerase (TaKaRa, Dalian, China) and the pKa Cloning Vector (Tiangen, Beijing, China). The recombinant plasmids (pKa-GA-related-genes) were transformed into *Escherichia coli* TOP10 competent cells, which were then cultured on LB agar medium supplemented with ampicillin (Amp) for selection.

Positive clones were identified by colony PCR, and putative positive clones were further propagated in liquid LB medium. Plasmids (pLB-GA-related-genes) were extracted using the Plasmid Miniprep Kit (Tiangen, Beijing, China) and verified by plasmid PCR. Both colony PCR and plasmid PCR were performed using Premix Taq™ (TaKaRa, Dalian, China) following the manufacturer's protocol, with the following conditions: 94 ℃ for 2 min, followed by 35 cycles of 94 ℃ for 30 s, 60 ℃ for 30 s, and 72 ℃ for 2. 5 min, and a final extension at 72 ℃ for 5 min. The PCR products were confirmed by agarose gel electrophoresis. Plasmids with positive verification were sent for sequencing. All primers used in this experiment are listed in Supply: Appendix table 2.

1. 6 Bioinformatics analysis

Based on the full-length cDNA sequences, open reading frame (ORF) prediction, conserved domain (CD) analysis, and multiple sequence alignment were

performed using online tools: ORF Finder (https://www. ncbi. nlm. nih. gov/orffinder/), Conserved Domain Database (CDD,https://www. ncbi. nlm. nih. gov/Structure/cdd/wrpsb. cgi), and BLAST (https://blast. ncbi. nlm. nih. gov/Blast. cgi), respectively. Motif identification was conducted using the online MEME Suite (https://meme-suite. org/meme/index. html) and TBtools software.

1. 7 cDNA synthesis and qPCR analysis

cDNA was synthesized using the FastKing Reverse Transcription System (TIANGEN Biotech, Beijing, China). Quantitative real-time PCR (qPCR) was performed with the SYBR® Green Pro Taq HS qPCR Kit (Accurate Biology, Hunan, China) in a 20 μL reaction volume on an ABI 7500 System (Thermo, Massachusetts, USA), following the manufacturers' protocols. The qPCR conditions were as follows: initial denaturation at 95 ℃ for 10 s, followed by 40 cycles of 95 ℃ for 3 s and 60 ℃ for 10 s. *EF-1-α* and *TUA* were used as internal reference genes. All experiments included three biological replicates and three technical replicates. qPCR results were analyzed using the $2^{-\Delta\Delta Ct}$ method (Zhu et al. , 2018). The primers used for qPCR are listed in Supply: Appendix table 2.

1. 8 Statistical analysis

Statistical analyses were performed using SPSS 23 software. The Shapiro-Wilk test was used to assess data normality. For normally distributed data, one-way analysis of variance (ANOVA) was used to evaluate significant differences among groups: The Bonferroni test was applied for data with homogeneous variances, while Dunnett's T3 test was used for data with heterogeneous variances. Nonparametric tests were employed for non-normally distributed data. Graphs and bar charts were generated using GraphPad Prism 8. 3. 0 software. The growth dynamics of fruit phenotypic parameters were fitted using the Logistic equation model (Baar et al. , 2024). Correlation analyses between gene expression levels and phenotypic traits were performed in R (version 2024. 12. 1+563) using the tidyverse, Hmisc, and corrplot packages.

2 Results

2. 1 Fruit growth and development pattern

2. 1. 1 Morphological development process of *A. villosum* fruits The infructescence of *A. villosum* typically develop as sequential capsule clusters along the inflorescence axis. Fig. 1−4 illustrate the morphological characteristics of *A. villosum* fruits and seeds at different developmental stages. Individual fruits are ellipsoidal capsules composed of a pericarp and enclosed seeds, with surface ornamentation characterized by short spines that emit volatile aromatic compounds.

Morphometric analysis revealed that fruits exhibited a nearly cylindrical morphology at 0 DAP, undergoing a gradual transition to an elliptical shape throughout the entire growth period. Notably, spine differentiation initiated at 6 DAP, displaying initial red pigmentation that intensified to purplish red during maturation. Seeds, initially encapsulated by white septal membranes, consolidated into densely packed aggregates by 18 DAP. A two-phase color transition was observed during seed development: Seeds maintained an ivory-white coloration until 60 DAP, followed by melanin-mediated blackening at 75 DAP.

2. 1. 2 Dynamic changes in fruit and seed growth-related mass parameters Both fruit and seed growth-related mass parameters, including transverse diameter, longitudinal diameter, fresh weight, volume, and pericarp development, exhibited characteristic sigmoidal patterns (slow-fast-slow phases) (Fig. 5). Notably, seed mass accounted for less than 50% of the total fresh weight of fruits throughout the developmental period. The transverse diameter growth rate exceeded the longitudinal diameter growth rate between 0−12 DAP (transverse/longitudinal diameter ratio < 1), while both dimensions grew at similar rates after 12 DAP (Fig. 5a). Fruit peel thickness (FPT), fruit thorn length (FTL), and seed size exhibited single growth peaks: FPT peaked at 24 DAP, FTL at 27 DAP, and seed size at 30 DAP (Fig. 5b−d).

2. 1. 3 Logistic model fitting and multivariate analysis of growth parameters Logistic equations provided good curve fitting for all growth parameters, with

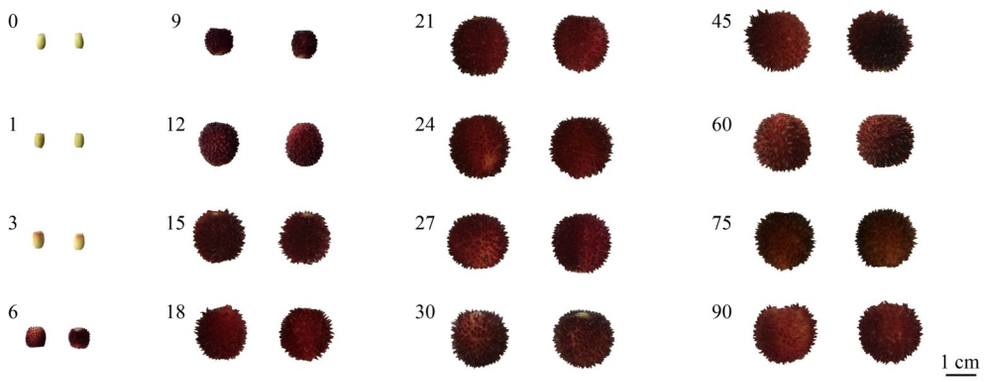

Numbers in the figure indicate days after pollination (DAP).

Fig. 1 Morphological characteristics of *A. villosum* fruits at different developmental stages

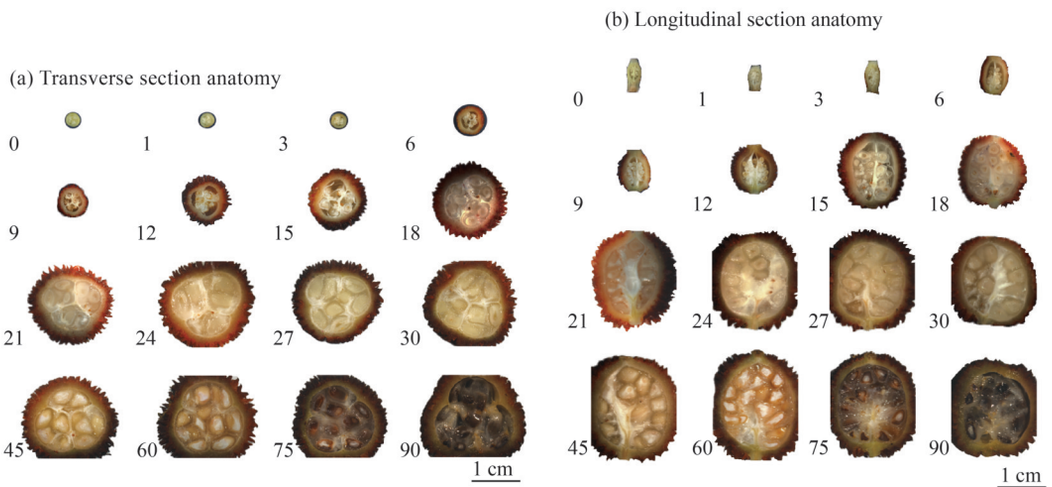

Numbers in the figure indicate days after pollination (DAP).

Fig. 2 Anatomical characteristics of *A. villosum* fruit sections at different developmental stages

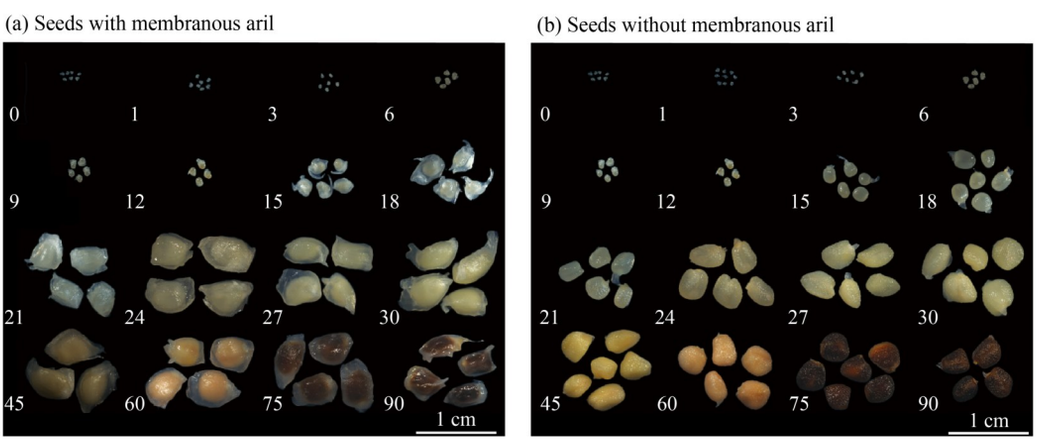

Numbers in the figure indicate days after pollination (DAP).

Fig. 3 Morphological characteristics of *A. villosum* seeds at different developmental stages

correlation coefficients (r) ranging from 0.796 5 to 0.978 2 (Table 1). The growth rates of fruit fresh weight, seed mass, and seed size were closely aligned. The developmental peaks of fruit transverse

Numbers in the figure indicate days after pollination (DAP).

Fig. 4 Dynamic changes in seed mass of *A. villosum* at different developmental stages

diameter (FTD), fruit longitudinal diameter (FLD), fruit peel thickness (FPT), and fruit thorn length (FTL) occurred earlier than seed weight accumulation, indicating that post-maturation dry matter accumulation is the primary determinant of final fruit weight. The fruit abscission rate peaked between 12−15 DAP, coinciding with the rapid growth of fruit volume and mass. The fruit abscission rate has been documented in previous studies (LÜ et al. , 2021).

Pearson correlation analysis revealed positive correlations among all measured traits ($r \geqslant 0.61$) (Fig. 6). Notably, strong positive associations were observed between fruit fresh weight and seed size ($r=0.89$), seed mass ($r=0.88$), transverse/longitudinal diameter ratio ($r=0.87$), and fruit thorn length ($r=0.86$). The fruit abscission rate exhibited significantly positive correlations with all growth parameters ($P<0.05$). Previous studies have linked fruit abscission to nutrient depletion and hormonal imbalance during rapid growth phases, which may be attributed to increased metabolic demands.

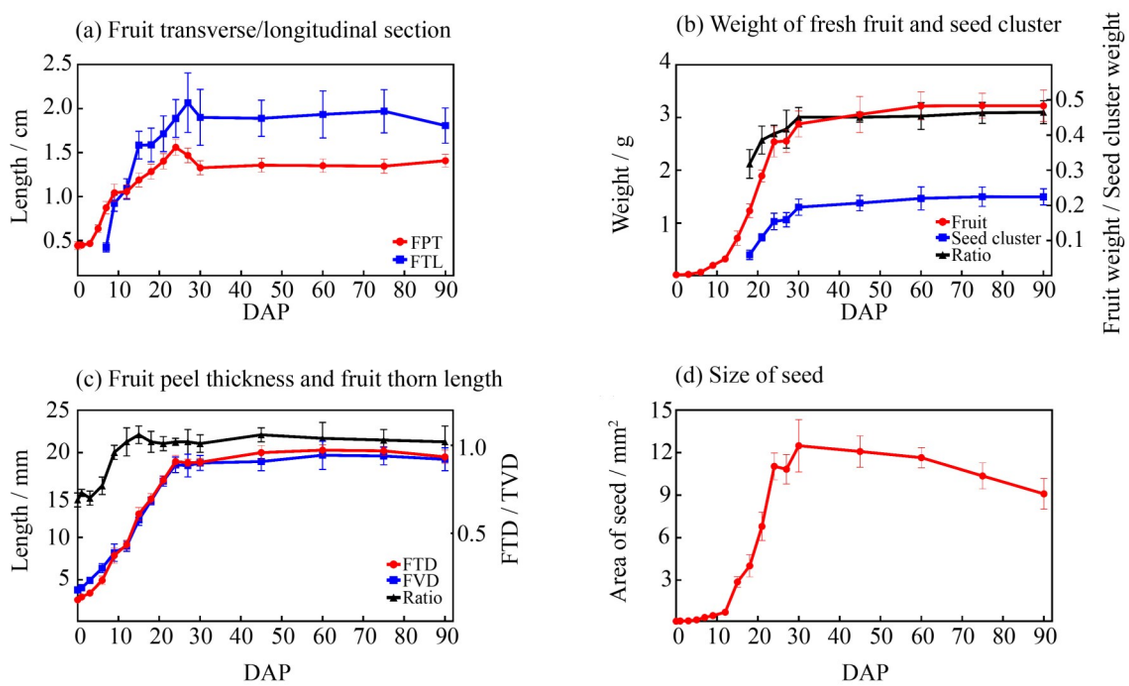

Data are presented as mean ± standard deviation (SD) ($n \geqslant 3$).

Fig. 5 Dynamic changes in fruit-related characteristics during *A. villosum* fruit growth and development

2. 2 Expression patterns of GA-related genes during fruit development

2. 2. 1 Selection, cloning, and bioinformatics analysis of GA-related genes RNA quality is presented in Supply: Appendix table 1. Additionally, based on our previous transcriptome database studies of filaments/styles and fruit abscission zones (He, 2020; Yang et al. , 2022), 10 candidate GA-related genes were selected (Supply: Appendix table 4). To obtain the full-length cDNA sequences of these GA-related genes, one-step RT-PCR and RACE-PCR were performed. After sequencing, the 3' and 5' cDNA sequences

Table 1 Logistic model of fruit growth indexes of *A. villosum* [1)]

Index	Equation	r	t_1	t_2	t_3
Fresh fuit weight	$Y=3.154/(1+162.4450e^{-0.2602x})$	0.978 2	14	20	25
Fresh seed cluster weight	$Y=1.457/(1+160.4127e^{-0.2375x})$	0.843 8	16	21	27
Seed size	$Y=11.260/(1+1\,891.0358e^{-0.3992x})$	0.957 0	16	19	22
FTD	$Y=20.100/(1+8.1983e^{-0.1746x})$	0.988 6	5	12	20
FLD	$Y=19.720/(1+5.3019e^{-0.1492x})$	0.968 9	2	11	20
FPT	$Y=1.402/(1+6.9257e^{-0.2096x})$	0.921 9	3	9	16
FTL	$Y=1.920/(1+15.6089e^{-0.2627x})$	0.796 5	5	10	15
Fruit dropping rate	$Y=63.170/(1+83\,194.3736e^{-0.8423x})$	0.869 5	12	13	15

1) r is goodness-of-fit index; t_1, t_2 and t_3 are the three key inflection points of Logistics curve, representing the days of slow growth phase, rapid growth period and mature period, respectively.

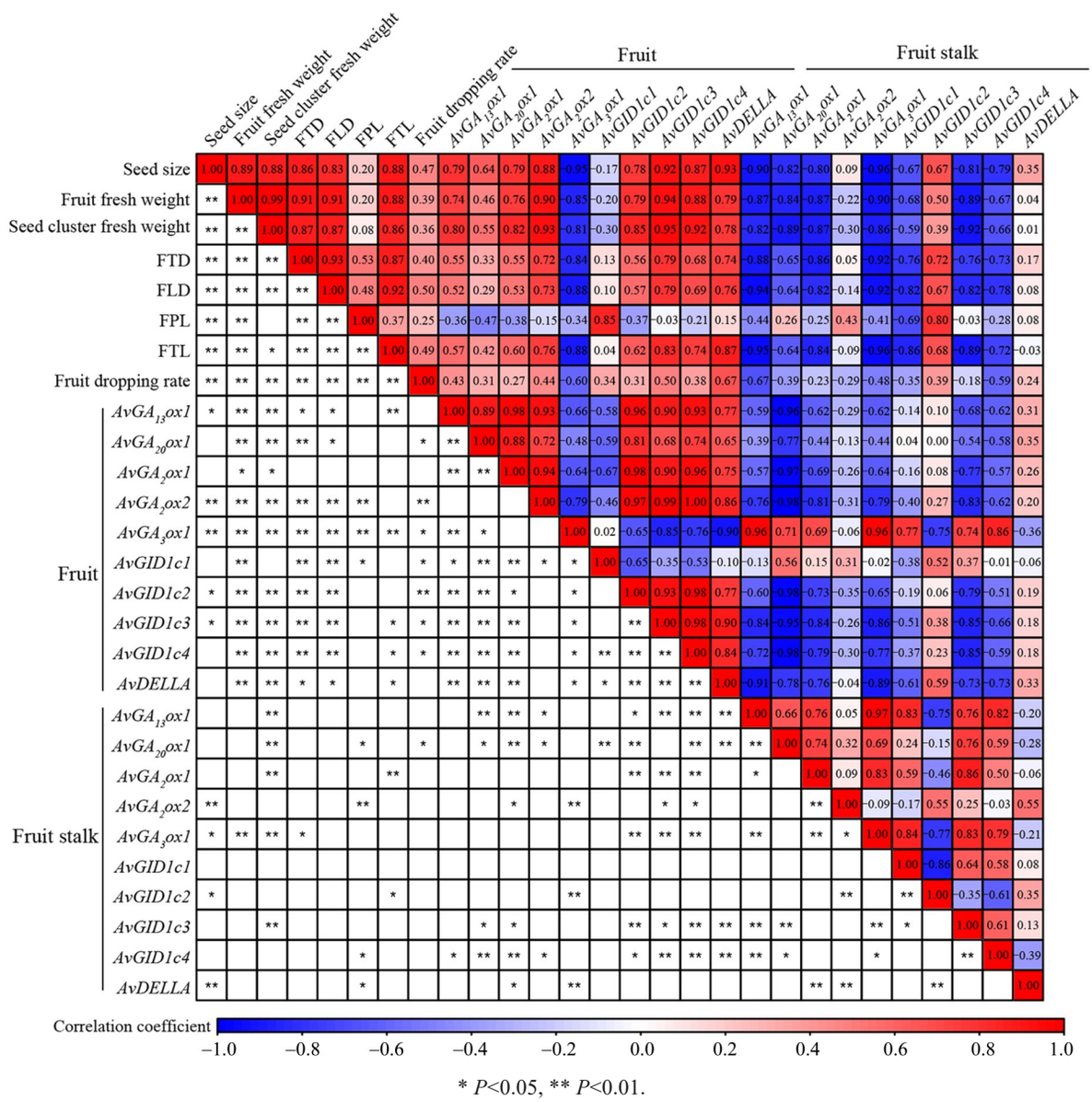

Fig. 6 Correlation analysis between phenotypic traits during *A. villosum* fruit growth and development and expression levels of gibberellin (GA)-related genes

were spliced using DNAMAN software, resulting in 10 full-length GA-related cDNA sequences. Subsequently, phylogenetic tree and motif analyses revealed that these 10 GA-related genes share high homology with their orthologs from other plant species (Supply: Appendix fig. 1). The GA-related gene sequences reported in this study are available in the NCBI GenBank database under the following accession IDs: ON186100.1, ON186101.1, ON186102.1, ON186103.1,ON186104.1,ON186105.1,ON186106.1, ON186107.1,ON186108.1,ON186109.1.

2. 2. 2 Expression patterns of GA-related genes during fruit development To clarify the molecular basis of GA level fluctuations during fruit development, the relative expression levels of GA-related genes were analyzed(Fig. 7). After artificial pollination(0−6 DAP), the expression levels of GA-related genes in fruit stalks at 6 DAP were significantly higher than those at 0 DAP, except for *AvGID1c1*—this may be compensated by *AvGID1c2*, *3*, and *4*. In contrast, the expression levels of GA-related genes in fruits at 6 DAP showed downregulation or no significant change compared with those at 0 DAP.

During 6−12 DAP, the expression levels of GA-related genes in fruit stalks at 12 DAP were lower than those at 6 DAP. Notably, *AvGA$_3$ox1* expression in fruits reached its peak at this stage. During 12−18 DAP, *AvGA$_{13}$ox1*, *AvGA$_{20}$ox1*, *AvGA$_3$ox1*, and *AvGID1c1*,*3*,*4* reached their peak expression levels in fruit stalks; increased expression of *AvGA$_{13}$ox1* was also observed in fruits during this period.

During 18−24 DAP, two GA signal transduction genes (*AvGID1c1* and *AvGID1c2*) were upregulated in fruits and fruit stalks, respectively. During 24−30 DAP, only *AvGID1c1* was upregulated in fruit stalks. After 30 DAP, *AvGA$_3$ox1* expression showed no significant change, while other GA-related genes exhibited a gradual upward trend.

2. 2. 3 Correlation between GA-related gene expression and phenotypic traits The expression patterns of GA pathway genes significantly influenced fruit morphology. Pearson correlation analysis revealed that most GA-related genes exhibited positive correlations with various growth parameters (Fig. 6). Notably, *AvGA$_3$ox1*—a key enzyme catalyzing active GA biosynthesis—showed significantly negative correlations with both fruit fresh weight (r=−0. 73, P<0. 01) and fruit abscission rate (r= − 0. 68, P<0. 05). This may reflect the plant's precise spatiotemporal regulation of hormone synthesis rather than a simple inhibitory relationship, suggesting distinct stage-specificity in fruit growth wherein the primary role of *AvGA$_3$ox1* is likely concentrated in the growth initiation phase.

In contrast, most GA-related genes in fruit stalks displayed negative correlations with growth parameters. However, the GA signal transduction gene *AvGID1c* was highly expressed in fruit stalks, with its expression level showing significantly positive correlations with seed size (r=0. 79, P<0. 01) and fruit thorn length (FTL) (r=0. 75, P<0. 05).

3 Discussion

A. villosum inflorescence typically bears 7−13 florets, and theoretically, each floret can develop into a fruit under optimal pollination and resource conditions. However, extensive fruit abscission critically constrains final yield, reducing the number of productive fruits to fewer than 3 per inflorescence. Although farmers adopt various agricultural practices to mitigate fruit drop, evidence-based precision management protocols remain underdeveloped. Notably, the inappropriate application of fruit-retention fertilizers has paradoxically exacerbated abscission rates, severely impacting cultivation profitability. These observations highlight the critical need to elucidate the mechanisms underlying fruit abscission to improve *A. villosum* yields.

Gibberellins (GAs) play pivotal roles in regulating fruit morphogenesis, developmental progression, and abscission. In tomato, the expression level of the *GA$_{20}$ox* gene in pollinated ovaries is significantly higher than that in unpollinated ovaries, which likely promotes the biosynthesis of active GAs (Carlos et al., 2007). In Arabidopsis, fertilization triggers GA synthesis in the ovule (Dorcey et al., 2009). However, in our study, the expression of GA-related genes in *A. villosum* fruits exhibited an initial decline after pollination, followed by a gradual increase. Interestingly, fruit stalk tissues showed

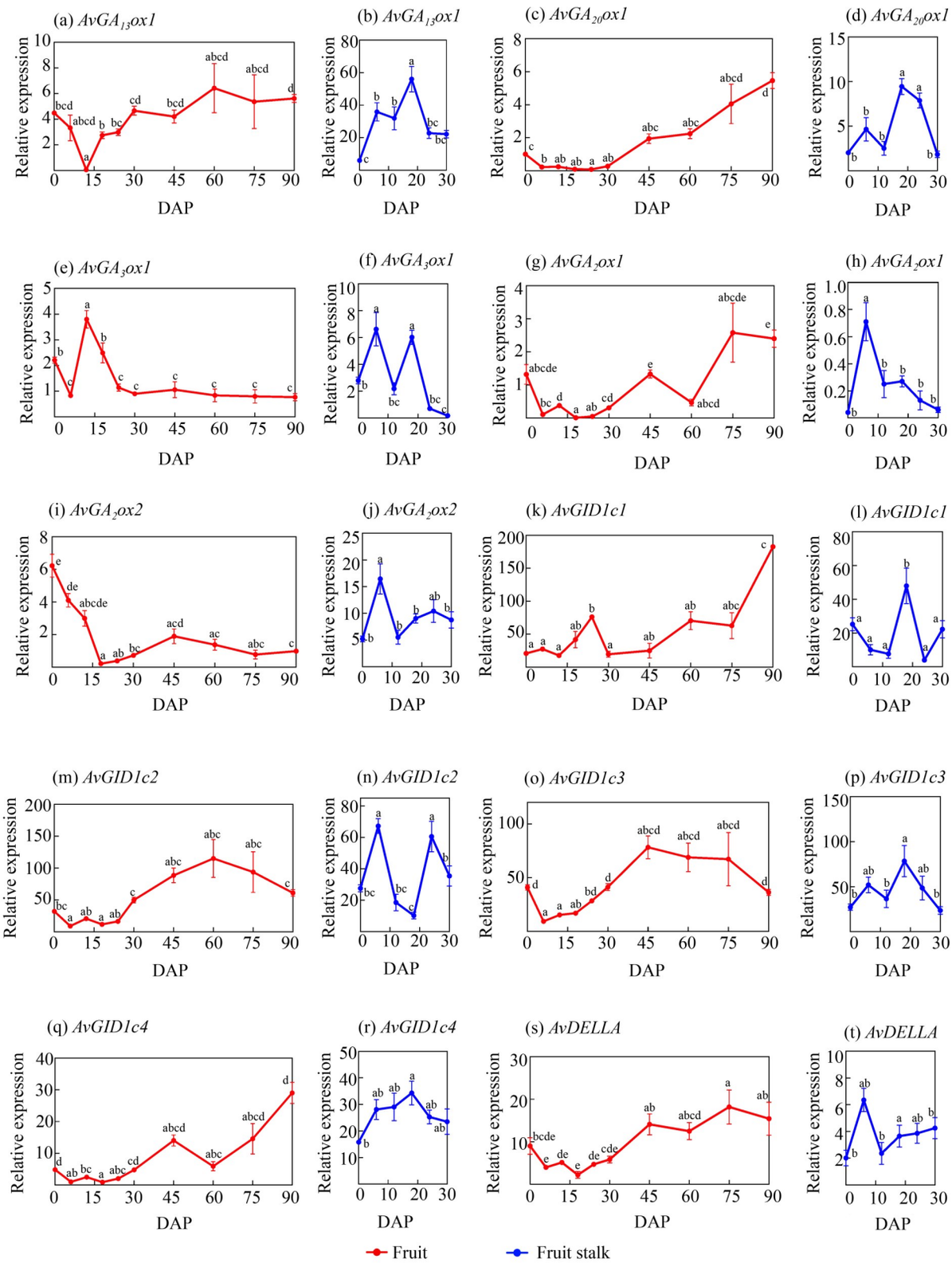

Data are presented as mean ± standard deviation (SD) (n=3).

Different lowercase letters indicate significant differences (P<0.05, one-way analysis of variance [ANOVA]).

Fig. 7 Relative expression levels of gibberellin (GA)-related genes in *A. villosum* fruits (red curves) and fruit stalks (blue curves)

elevated expression of *AvGA$_{13}$ox1*, *AvGA$_3$ox1*, and *AvGID1c2*.

Previous studies have proposed that the fruit stalk (pedicel) serves as a critical organ connecting the source and sink in plants, facilitating nutrient transport (Xiao et al. , 2021; Li et al. , 2019a). For instance, elevated GA concentrations in waxberry pedicels effectively reduce fruit abscission (Zhang et al. , 2019). In apple, high concentrations of GAs and nutrients in the fruit stalk enhance fruit sink activity, thereby improving the efficiency of assimilate transport to the fruit (Sha et al. , 2020). Consistent with these findings, GA-related genes in *A. villosum* were more actively expressed in the fruit stalk than in the fruit itself. The high expression of GA-related genes in the pedicel may enhance GA sensitivity or promote the synthesis of active GAs, thereby maintaining pedicel physiological activity, facilitating directional nutrient transport, and strengthening fruit sink competitiveness.

Furthermore, our results align with previous reports that elevated GA_3 concentrations in pedicels exert fruit-retention effects (LÜ et al. , 2021). This spatial divergence in gene expression suggests that compensatory GA accumulation in the pedicel may counteract insufficient GA signaling in the fruit, providing a potential mechanism for regulating *A. villosum* fruit abscission.

GAs play a critical role in early fruit development (Fenn et al. , 2021). In black pepper, *GA$_{20}$ox* expression exhibits high activity during the early stages of fruit growth, while the levels of GA_1 and GA_4 begin to increase from the fruit set phase and peak throughout the fruit growth period (Khew et al. , 2020). In tomato, overexpression of *GA$_2$ox1* leads to the downregulation of cell expansion-related genes, resulting in reduced cell volume, decreased fruit weight, and fewer seeds (Chen et al. , 2016). Notably, a significant negative correlation was observed between *AvGA$_3$ox1* expression and *A. villosum* fruit development (Fig. 6).

GA$_3$ox is a key enzyme in the biosynthesis of active GAs. For instance, in tomato, the expression level of *SlGA$_3$ox1* and the GA_4 concentration peaked simultaneously at the mature green stage; thereafter, increased *GA$_2$ox* gene expression were accompanied by decrease in both GA_4 concentration and *SlGA$_3$ox1* transcript abundance (Li et al. , 2019b). This pattern is consistent with the expression of *AvGA$_3$ox1* during 6−24 DAP, which may indicate high GA_4 concentrations during this period. The high expression of *AvGA$_3$ox1* was concentrated in early stages, potentially associated with initiating cell division or early fruit set (Shinozaki et al. , 2020). During the rapid fruit expansion stage (12−30 DAP), *AvGA$_3$ox1* expression was downregulated, which may reflect reduced GA synthesis. In tomato, decreased GA concentrations promote early fruit ripening (Li et al. , 2019b).

Based on these observations, we propose the following hypothesis: During early *A. villosum* fruit development, high *AvGA$_3$ox1* expression promotes the accumulation of bioactive GAs, thereby enhancing fruit set and early development. Subsequently, a 'braking mechanism' is activated during the rapid growth phase, reducing GA synthesis to prepare the fruit for the subsequent maturation stage.

Beyond GA signaling, auxin, ethylene, and brassinosteroids pathways collectively regulate fruit development. For instance, application of 3, 5, 6-TPA and 2, 4-D increased the average fruit diameter of citrus (Mesejo et al. , 2003). Silencing *LeEIN2* in tomato delayed fruit development and ripening (Zhu et al. , 2006). Exogenous brassinosteroid application to grape berries significantly promoted ripening (Symons et al. , 2006). Future interventions targeting exogenous hormone application before fruit abscission could potentially synchronize fruit growth demands with nutrient allocation, thereby mitigating abscission and enhancing *A. villosum* yield.

While this study has elucidated the developmental dynamics of *A. villosum* fruits and the spatiotemporal expression patterns of GA-related genes, substantial work remains for future research, including: (i) comprehensive profiling of endogenous hormone levels (e. g. , GA_3, ethylene, and auxin) to decipher their temporal dynamics during fruit development and abscission; (ii) establishment of a stable genetic transformation system for *A. villosum* to enable functional

genomics studies; (iii) functional validation of candidate genes (e. g., *AvGA$_3$ox*, *AvGID1c*) through CRISPR/Cas9-mediated knockout or overexpression to confirm their roles in fruit development.

4 Conclusion

This study elucidated the fruit growth dynamics of *A. villosum* and the spatiotemporal expression patterns of GA-related genes. The fruit abscission rate showed strong positive correlations with key fruit growth parameters, including fresh weight, transverse/longitudinal diameters, seed size, and fruit thorn length (FTL). Crucially, GA biosynthesis and signaling genes were closely associated with both fruit development and abscission. Based on the GA-related gene expression patterns identified herein, we propose that exogenous application of gibberellic acid during the early phase of *A. villosum* fruit development may be strategically integrated into horticultural management practices to mitigate premature fruit abscission and improve yield in plantations.

References:

ALFEREZ F, de CARVALHO D U, BOAKYE D, 2021. Interplay between abscisic acid and aibberellins, as related to ethylene and sugars, in regulating maturation of non-climacteric fruit[J]. Int J Mol Sci, 22(2): 669.

ARIIZUMI T, SHINOZAKI Y, EZURA H, 2013. Genes that influence yield in tomato[J]. Breed Sci, 63(1): 3-13.

BAAR S, KOBAYASHI Y, HORIE T, et al, 2024. A logistic model for precise tomato fruit-growth prediction based on diameter-time evolution[J]. Comput Electron Agric, 227: 109500.

BAI Q, HUANG Y, SHEN Y Y, 2021. The physiological and molecular mechanism of abscisic acid in regulation of fleshy fruit ripening[J]. Front Plant Sci, 11: 619953.

BINENBAUM J, WEINSTAIN R, SHANI E, 2018. Gibberellin localization and transport in plants[J]. Trends Plant Sci, 23(5): 410-421.

CARLOS S J, SANJUÁN R, RUIZ-RIVERO O, et al, 2007. Gibberellin regulation of fruit set and growth in tomato [J]. Plant Physiol, 145(1): 246-257.

CHEN S, WANG X J, ZHANG L Y, et al, 2016. Identification and characterization of tomato gibberellin 2-oxidases (GA2oxs) and effects of fruit-specific *SlGA2ox1* overexpression on fruit and seed growth and development[J]. Hortic Res, 3: 16059.

CHEN W W, 2010. Lingnan materia medica [M]. Guangzhou: Guangdong Science & Technology Press: 297-328.

CSUKASI F, OSORIO S, GUTIERREZ J R, et al, 2011. Gibberellin biosynthesis and signalling during development of the strawberry receptacle[J]. New Phytol, 191 (2): 376-390.

de BOER H, NEWMAN M, POULSEN A D, et al, 2018. Convergent morphology in alpinieae (Zingiberaceae): Recircumscribing *Amomum* as a monophyletic genus[J]. TAXON, 67(1): 6-36.

DORCEY E, URBEZ C, BLÁZQUEZ M A, et al, 2009. Fertilization-dependent auxin response in ovules triggers fruit development through the modulation of gibberellin metabolism in *Arabidopsis*[J]. Plant J, 58(2): 318-332.

ESTORNELL L H, AGUSTÍ J, MERELO P, et al, 2013. Elucidating mechanisms underlying organ abscission[J]. Plant Sci, 199: 48-60.

FENG Y L, LI X, 2007. The combined effects of soil moisture and irradiance on growth, biomass allocation, morphology and photosynthesis in *Amomum villosum* [J]. Agrofor Syst, 71(2): 89-98.

FENN M A, GIOVANNONI J J, 2021. Phytohormones in fruit development and maturation[J]. Plant J, 105(2): 446-458.

GAO S P, CHU C C, 2020. Gibberellin metabolism and signaling: Targets for improving agronomic performance of crops[J]. Plant Cell Physiol, 61(11): 1902-1911.

GARCÍA-ROJAS M, MENESES M, OVIEDO K, et al, 2018. Exogenous gibberellic acid application induces the overexpression of key genes for pedicel lignification and an increase in berry drop in table grape[J]. Plant Physiol Biochem, 126: 32-38.

GILLASPY G, BEN-DAVID H, GRUISSEM W, 1993. Fruits: A developmental perspective [J]. Plant Cell, 5 (10): 1439-1451.

GUO Y H, YUAN C, TANG L, et al, 2016. Responses of clonal growth and photosynthesis in *Amomum villosum* to different light environments[J]. Photosynthetica, 54(3): 396-404.

HAN D C, HUANG Q C, FANG M K, et al, 1984. The influence of different shading conditions on the water regime and fruit yield in *Amomum villosum* Lour. plantation[J].

Acta Sci Nat Univ Sunyatseni, 23(3): 10−15.

HE Z H, 2020. Transcriptome analysis of fruitlet abscission related genes in *Amomum villosum* [D]. Guangzhou: Guangzhou University of Chinese Medicine.

HEDDEN P, 2020. The current status of research on gibberellin biosynthesis[J]. Plant Cell Physiol, 61(11): 1832−1849.

HU J H, ISRAELI A, ORI N, et al, 2018. The interaction between DELLA and ARF/IAA mediates crosstalk between gibberellin and auxin signaling to control fruit initiation in tomato[J]. Plant Cell, 30(8): 1710−1728.

HU Z Y, LAN S R, ZHAO N, et al, 2019. Soft−X−irradiated pollens induce parthenocarpy in watermelon *via* rapid changes of hormone−signalings and hormonal regulation [J]. Sci Hortic, 250: 317−328.

HUANG L Q, GUO L P, ZHAN Z L, 2020. Standard collection of daodi herbs [M]. Beijing: Beijing Science and Technology Publishing: 781−787.

KHEW C Y, MORI I C, MATSUURA T, et al, 2020. Hormonal and transcriptional analyses of fruit development and ripening in different varieties of black pepper (*Piper nigrum*)[J]. J Plant Res, 133(1): 73−94.

LI H, FAN Y W, ZHI H, et al, 2019a. Influence of fruit stalk on reactive oxygen species metabolism and quality maintenance of peach fruit under chilling injury condition[J]. Postharvest Biol Technol, 148: 141−150.

LI H, WU H, QI Q, et al, 2019b. Gibberellins play a role in regulating tomato fruit ripening[J]. Plant Cell Physiol, 60(7): 1619−1629.

LI Z K, LUO X, YAO Y L, et al, 2024. Integrated analysis of metabolomics, flavoromics, and transcriptomics for evaluating new varieties of *Amomum villosum* Lour [J]. Plants, 13:(17): 2382.

LIAO X, LI M S, LIU B, et al, 2018. Interlinked regulatory loops of ABA catabolism and biosynthesis coordinate fruit growth and ripening in woodland strawberry [J]. Proc Natl Acad Sci USA, 115(49): E11542−E11550.

LIU L L, WANG Z G, LIU J L, et al, 2018. Histological, hormonal and transcriptomic reveal the changes upon gibberellin−induced parthenocarpy in pear fruit [J]. Hortic Res, 5: 1.

LIU Y, LI Y, GUO H X, et al, 2023. Gibberellin biosynthesis is required for CPPU−induced parthenocarpy in melon [J]. Hortic Res, 10(6): uhad084.

LÜ B D, HU J J, TANG L Y, et al, 2021. The study on the fruit dropping law and physiological mechanism of *Amomum villosum*[J]. Plant Physiol J, 57(2): 429−438.

MESEJO C, MARTÍNEZ−FUENTES A, JUAN M, et al, 2003. Vascular tissues development of *Citrus* fruit peduncle is promoted by synthetic auxins [J]. Plant Growth Regul, 39(2): 131−135.

PENG G T, HUANG S Z, FU J R, et al, 2003. The preliminary studies of storage and germination characters of seeds of *Ardisia* spp[J]. Acta Sci Nat Univ Sunyatseni, 42(4): 79−83.

PHOKAS A, COATES J C, 2021. Evolution of DELLA function and signaling in land plants[J]. Evol Dev, 23(3): 137−154.

REIG C, MARTÍNEZ−FUENTES A, MESEJO C, et al, 2018. Hormonal control of parthenocarpic fruit set in 'Rojo Brillante' persimmon (*Diospyros kaki* Thunb.)[J]. J Plant Physiol, 231: 96−104.

SEYMOUR G B, GRANELL A, 2014. Fruit development and ripening[J]. J Exp Bot, 65, (16): 4489−4490.

SHA J C, WANG F, XU X X, et al, 2020. Studies on the translocation characteristics of ^{13}C−photoassimilates to fruit during the fruit development stage in 'Fuji' apple [J]. Plant Physiol Biochem, 154, 636−645.

SHINOZAKI Y, BEAUVOIT B P, TAKAHARA M, et al, 2020. Fruit setting rewires central metabolism via gibberellin cascades[J]. Proc Natl Acad Sci USA, 117(38): 23970−23981.

SU P, TONG Y R, CHENG Q Q, et al, 2016. Functional characterization of ent−copalyl diphosphate synthase, kaurene synthase and kaurene oxidase in the Salvia miltiorrhiza gibberellin biosynthetic pathway [J]. Sci Rep, 6: 23057.

SYMONS G M, DAVIES C, SHAVRUKOV Y, et al, 2006. Grapes on steroids. brassinosteroids are involved in grape berry ripening[J]. Plant Physiology, 140(1): 150−158.

TANG L, VASHISTH T, 2020. New insight in Huanglongbing−associated mature fruit drop in *Citrus* and its link to oxidative stress[J]. Sci Hortic, 265: 109246.

TAYLOR J E, WHITELAW C A, 2001. Signals in abscission [J]. New Phytol, 151(2): 323−340.

WANG Y J, ZHAO J, LU W J, et al, 2017. Gibberellin in plant height control: old player, new story[J]. Plant Cell Rep, 36(3): 391−398.

XIANG H Y, OKAMURA H, KEZUKA Y, et al, 2018. Physical and thermodynamic characterization of the rice gibberellin receptor/gibberellin/DELLA protein complex [J]. Sci Rep, 8(1): 17719.

XIAO Z Y, CHIN S, WHITE R G, et al, 2021. Vascular connections into the grape berry: The link of structural investment to seededness[J]. Front Plant Sci,12: 662433.

XIE R J, GE T, ZHANG J, et al, 2018. The molecular events

of IAA inhibiting *Citrus* fruitlet abscission revealed by digital gene expression profiling [J]. Plant Physiol Biochem, 130: 192−204.

XU J, LI M X, SU J, et al, 2018. Study on ecological stereoscopic cultivation mode of *Amomum villosum*−*Dimocarpus longan* [J]. China J Chin Mater Med, 43 (2): 288−298.

XU P P, HU J B, CHEN H Y, et al, 2023. SMAX1 interacts with DELLA protein to inhibit seed germination under weak light conditions via gibberellin biosynthesis in *Arabidopsis*[J]. Cell Rep, 42(7): 112740.

YAMAGUCHI S, 2008. Gibberellin metabolism and its regulation[J]. Annu Rev Plant Biol, 59: 225−251.

YAMAMURA Y, TAGUCHI Y, ICHITANI K, et al, 2018. Characterization of ent−kaurene synthase and kaurene oxidase involved in gibberellin biosynthesis from *Scoparia dulcis*[J]. J Nat Med, 72(2): 456−463.

YANG B H, XU J, TANG L Y, et al, 2022. Transcriptome sequencing and bioinformatics analysis of filaments and styles of *Amomum villosum* [J]. Jiangsu Agric Sci, 50 (22): 38−45.

ZHANG S W, LIANG S M, ZHENG X L, et al, 2019. The relationship between changes of endogenous hormones and pre−harvest fruit dropping of Chinese bayberry during fruit development [J]. Plant Physiol J, 55 (08): 1267−1275.

ZHANG Y J, NIE C R, ZHANG J W, et al, 2023. A gibberellin−responsive transcription factor from *Phalaenopsis* 'Big Chili' (PIF4) promotes flowering in *Arabidopsis thaliana*[J]. Plant Growth Regul, 101(2): 361−371.

ZHAO H Y, LI M, ZHAO Y Y, et al, 2021. A comparison of two monoterpenoid synthases reveals molecular mechanisms associated with the difference of bioactive monoterpenoids between *Amomum villosum* and *Amomum longigulare*[J]. Front Plant Sci, 12: 695551.

ZHU H L, ZHU B Z, SHAO Y, et al, 2006. Tomato fruit development and ripening are altered by the silencing of LeEIN2 gene [J]. J Integr Plant Biol, 48 (12): 1478−1485.

ZHU X H, DING T B, XU K K, et al, 2018. Cloning and expression analysis of two carboxylesterase genes in the cigarette beetle, *Lasioderma serricorne*[J]. Acta Sci Nat Univ Sunyatseni, 57(4): 136−144.

阳春砂果实发育过程中的表观性状变化与赤霉素相关基因的表达模式

吕秉鼎[1]，张玉仪[1,2]，汤丽云[3]，胡佳佳[1,4]，苏景[5]，徐杰[1,6]，何卓航[1,7]，何国振[1]

1. 广州中医药大学中药学院，广东 广州 510006
2. 华南农业大学资源环境学院，广东 广州 510642
3. 华南农业大学生命科学学院，广东 广州 510642
4. 丰城市人民医院药学部，江西 丰城 331100
5. 阳春市农业试验场（阳春市春砂仁试验场），广东 阳春 529600
6. 广东一方制药有限公司 / 广东省中药配方颗粒企业重点实验室，广东 佛山 528244
7. 广州达安基因股份有限公司，广东 广州 510665

摘要：阳春砂（*Amomum villosum*）的果实具有极高的药食两用价值，但其落果率高，产量低。为探究果实生长发育规律，本研究系统观测了阳春砂果实发育过程中的表观性状变化，并分析了赤霉素（GA，gibberellin）相关基因在果实及果柄发育过程中的表达模式。结果表明，阳春砂子房从授粉至成熟约需 90 d，果实生长呈“慢−快−慢”趋势，鲜质量积累高峰出现在人工授粉后第 14~25 天。在授粉后第 27 天前，子房、果色、果皮厚度及果刺长度均发生显著变化。通过生物信息学分析，鉴定出 10 个赤霉素相关候选基因，包括 1 个 $GA_{13}ox$、1 个 $GA_{20}ox$、1 个 GA_3ox、2 个 GA_2ox、4 个 *GID1c* 和 1 个 *DELLA*。果实与果柄中赤霉素相关基因的表达与果实生长发育及落果显著相关。研究结果系统解析了阳春砂果实生长发育规律及赤霉素相关基因的表达特性，为深入探究基因功能及筛选调控落果的关键候选基因提供了理论依据

关键词：阳春砂；赤霉素；果实生长发育；基因表达模式；生物信息学

（责任编辑　张　冰）